RIO: A Pervasive RFID-based Touch Gesture Interface

Swadhin Pradhan
UT Austin
swadhin@cs.utexas.edu

Eugene Chai
NEC Labs America
eugene@nec-labs.com

Karthikeyan Sundaresan
NEC Labs America
karthiks@nec-labs.com

Lili Qiu
UT Austin
lili@cs.utexas.edu

Mohammad A. Khojastepour
NEC Labs America
amir@nec-labs.com

Sampath Rangarajan
NEC Labs America
sampath@nec-labs.com

ABSTRACT

In this paper, we design and develop Rio, a novel battery-free touch sensing user interface (UI) primitive for future IoT and smart spaces. Rio enables UIs to be constructed using off-the-shelf RFID readers and tags, and provides a unique approach to designing smart IoT spaces. With Rio, any surface can be turned into a touch-aware surface by simply attaching RFID tags to them. Rio also supports custom-designed RFID tags, and thus allows specially customized UIs to be easily deployed into a real-world environment.

Rio is built using the technique of *impedance tracking*: when a human finger touches the surface of an RFID tag, the impedance of the antenna changes. This change manifests as a change in the phase of the RFID backscattered signal, and is used by Rio to track fine-grained touch movement over both off-the-shelf and custom-built tags. We study this impedance behavior in-depth and show how Rio is a reliable UI primitive that is robust even within a multi-tag environment. We leverage this primitive to build a prototype of Rio that can continuously locate a finger during a swipe movement to within 3*mm* of its actual position. We also show how custom-design RFID tags can be built and used with Rio, and provide two example applications that demonstrate its real-world use.

KEYWORDS

RFID; Touch Interface; Mutual Coupling; Impedance Tracking

1 INTRODUCTION

The future of IoT demands seamless, intuitive interaction between users and smart devices. The vision is one of *smart spaces* (Fig. 1a), where sensing and actuation interfaces are embedded into common objects, and can be controlled through touch, voice command, or gestures. Examples of such input modalities include wireless gesture sensing [1–3] which converts everyday body motions into input, and capacitive touch [4, 5] which recognizes physical actuation between a user and the IoT device. Imagine if all these input modalities operate without the need for any built-in battery or power source, and are integrated into everyday devices such as cups, bowls, door knobs, mattresses, and built upon hardware so cheap and simple that it can be installed or discarded easily. Any physical space can be converted into a smart space simply by embedding such input interfaces. The possibilities for such an input primitive are clearly endless.

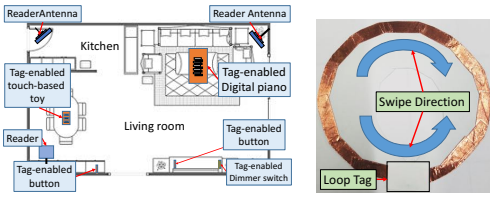

(a) Rio-enabled home setup. **(b) Custom Rio tag for volume control.**

Figure 1: Example applications of Rio.

Battery-Free Touch UI. We explore the design of a battery-free fine-grained touch gesture input interface using Radio Frequency IDentification (RFID) technology. RFIDs provide a low-cost, battery-free communication platform and have been used to develop sensing, activity recognition and localization solutions [6–11]. Among these notable works, machine learning techniques using the PHY-layer features of both off-the-shelf [8] and custom-built tags [9] have been successful in classifying several well-defined gestures such as hand waving, touching and swiping. Other approaches such as [12], have also designed custom backscatter capacitive measurement circuits to detect touch events on the tag antenna.

We note that these works only detect isolated, coarse-grained interactions and not fine-grained ones, such as the path traced by a finger over the surface of a tag. Machine learning approaches [8, 9] also demand a high training overhead that limits its deployability. For example, [8] uses 600 annotated interaction events to train and evaluate its classifier. and thus increase the cost and difficulty of large-scale integration into smart-spaces.

In this paper, we improve upon existing works by asking and answering an important question: *Can we use commercial off-the-shelf (COTS) RFIDs as a battery-free, low-cost, fine-grained touch-based user input primitive?*

We design and build such an input primitive using COTS RFID readers and tags. We call this primitive Rio, for **R**FID-based **I**nput / **O**utput. Rio turns COTS RFID tags into touch interfaces: a user interacts with Rio by touching the tag, and Rio accurately tracks the touch as it moves over the surface of a tag. Rio uses a novel technique of *impedance tracking* in backscatter communications. The human body is conductive, with a capacitance on the order

MobiCom '17, October 16-20, 2017, Snowbird, UT, USA

ACM ISBN 978-1-4503-4916-1/17/10…$15.00
https://doi.org/.1145/3117811.3117818

of hundreds of pico-Farads (*pF*) and a resistance of hundreds to thousands of Ohms [13, 14]. When a user touches an RFID tag, his/her body conductivity changes the effective *impedance* of the tag antenna. This impedance change manifests as a change in phase of the backscattered signal. Rio tracks this phase change to determine the location of the finger within a tag. By accurately modeling the relationship between impedance and RF phase, this fine-grained tracking can be achieved with minimal training overhead. Our evaluations show a tracking error of under 4% with only 4 training events (vs. 600 training events for IDSense [8]).

Rio offers three key features that make it ideal for IoT setting:

(i) Fine-Grained Accuracy. Rio detects finger taps on RFID tags with 100% accuracy, and tracks finger swipe positions to within 3*mm* of its true position (validated using a camera and OpenCV for finger tracking). This is achieved using off-the-shelf RFID tags, thus enabling a new battery-free, fine-grained and accurate UI primitive for smart-spaces.

(ii) Low-cost Hardware. Rio makes use of COTS RFID tags. We have tested Rio with a variety of tags, an example of which is the Monza 4D Dogbone tag [15]. These tags are extremely low-cost, and can be purchased for as low as 14-cents each. The low-cost nature of RFID tags lowers the barrier to smart spaces as large numbers of tags can be installed within an area easily.

(iii) Customizable User Interface. Rio also supports custom-designed RFID tags. We build tags with custom-shaped antennas by laying out the antennas with copper metal tape and inductively couple them to small near-field RFID tags. Rio tracks touch gestures over these custom antennas, and thus enables custom, application-specific interfaces to be built.

Applications. These features of Rio offer a novel primitive for future IoT UI design. As an example, RFID tags can be placed throughout a room to be used as dimmer switches — a user swipes his/her finger up and down a tag to increase/decrease the lighting brightness. A similar Rio interface can be used to increase/decrease the volume of audio systems. Rio also enables multiple tags to be arranged into an array. Such an array can be affixed to any table or wall to serve as a battery-free, wireless touch-pad to interact with home automation/entertainment systems.

Rio supports custom tags with antennas designed into application-specific control shapes. For example, a custom tag shown in Fig. 1b can be installed on a sofa to allow users to adjust the volume of the TV by swiping (anti-)clockwise over the tag. Such applications require fine-grained continuous touch tracking, which is now enabled by Rio. Rio thus opens up a whole new selection of such intuitive, battery-free interfaces that can be embedded into every-day spaces.

Contributions. In developing Rio as a practical, battery-free user-interface primitive, we address several challenges and make the following contributions:

(1) Rio as a Reliable Primitive for Touch Sensing. To validate the reliability of Rio's primitive, we present a detailed measurement study of RFID backscatter signals in response to physical touch across the RFID antenna. We use both over-the-air and Vector Network Analyzer (VNA) measurements, to show how (a) the impedance of the RFID antenna will vary in response to physical touch; (b) the amount of variation depends on the location of the physical contact with the antenna; and (c) the variations in antenna impedance form the dominant factor (compared to other artifact like multi-path) contributing to a corresponding change in the magnitude and phase of the backscattered signal. Equipped with this understanding, Rio uses this touch-dependent phase change behavior of RFID tags as a primitive to detect touches on a RFID tag, as well as to track the location of the finger during a swipe over the tag surface.

(2) Making Rio Resilient in a Multi-Tag Environment. Previous works have identified that *mutual coupling* between tags [16–19] has a significant impact on backscattered signal phase. Hence, when multiple RFID tags are deployed close together on the same surface, the backscattered phase is affected by both the physical contact with the RFID antenna, as well as mutual coupling affects, thereby substantially affecting the tracking accuracy. While previous works have made similar observations [16–19], the impact of such coupling has been overcome largely by building tolerance into the solution. In contrast, we take a more active approach to model and understand the impact of inter-tag coupling on our primitive. With the help of our measurement campaign and supporting model, we show that while coupling can affect the phase change behavior on a desired tag and hence its tracking accuracy, it contributes to a stable, predictable phase-change pattern in the neighboring tags. Thus, by leveraging the joint phase-change behavior across multiple tags, Rio translates the challenge of coupling into an opportunity to enhance the tracking accuracy even in multi-tag scenarios.

(3) Leveraging Rio's Primitive. We design algorithms that leverage the touch-based phase-change primitive in Rio as well as the inter-tag coupling behavior to track touches to an median error of only 3 and 7 *mm* in single and multi-tag settings respectively. Rio's algorithms provide the flexibility to operate at various points in the accuracy-latency trade-off curve, allowing for a reasonable loss in accuracy for a more responsive real-time tracking.

(4) Exploring Rio's Potential. The ability to go beyond COTS tags expands the scope of applications possible with Rio. Custom-designed RFID tags mimicking different shapes, characters, etc. allow battery-free interfaces to be customized for specific smart spaces use cases in Rio. We describe how these tags can be constructed, and extend the touch/gesture tracking algorithms in Rio to support tracking applications with these custom-designed tags.

(5) Realizing Rio in Practice. We develop a prototype of Rio, and demonstrate its touch and gesture tracking accuracy using both COTS and custom-designed RFID tags. We demonstrate the robustness of Rio through exhaustive real-world evaluations, and show that accurate tracking is maintained even at different tag angles and distances to the RFID reader. We also develop two sample applications using custom-designed RFID tags to highlight the flexibility and practicality of Rio.

Our evaluations demonstrate that Rio (a) detects a human touch event with 100% accuracy and (b) tracks the location of a human finger during a swipe gesture across the surface of a COTS RFID tag to within 3*mm* (less than 4% of the length of the RFID tag).

In the rest of this paper, we begin with a background on RFIDs in §2, followed by a quantitative and qualitative study of the RFID touch primitive in §3. We describe the algorithms for touch and swipe gesture tracking in §4, and extend it to support custom-designed RFID tags in §5. We then evaluate the Rio primitive in §6 and demonstrate two example applications in §6.4. Next, we discuss

a few points regarding the extensions and limitations of Rio in §7 and finally conclude in §9 after reviewing related works in §8.

2 PASSIVE RFID PRIMER

Passive RFID system communicates using a backscatter radio link, as shown in Fig. 2. The reader supplies a Continuous Wave (CW) periodic signal that persists indefinitely. The passive tags purely harvest energy from this CW signal. The tag then modulates its data on the backscatter signals using ON-OFF keying through changing the impedance on its antenna.

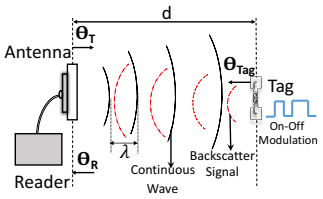

Figure 2: Operation of a RFID reader antenna and a tag.

Passive RFID tag: A typical passive RFID tag, as shown in Fig. 3b, consists of an antenna and an integrated circuit (chip). According to [20], passive RFID tag absorbs the most energy when the chip impedance and the antenna impedance are conjugately matched, *i.e.*, $Z_c = Z_a^*$ [21].

COTS RFID reader: COTS RFID reader [22] uses linear or circular polarized antennas for both transmitting and receiving. They generally provide facilities to access lower level information [23] like RSS and phase values etc. through SDK [24]. A COTS reader employs an open-loop estimation (*e.g.*, preamble correlation) or a closed-loop estimation technique for acquiring phase and RSS [25].

3 HUMAN TOUCH PRIMITIVE

Human touch on the RFID tag changes the effective impedance of the antenna, and will, in turn, influence the phase of the backscattered signal. In this section, we show how this phase-change behavior is used as a reliable and robust primitive for touch/gesture tracking in both single tag and multi-tag settings, and in the presence of artifacts such as multi-path and inter-tag coupling. We accomplish this with the help of both controlled and over-the-air measurements, and an analytical model that highlights the fundamental relationship between impedance change and RF phase.

3.1 How Does Human Touch Change the Backscatter Phase of a Single RFID Tag?

Fig. 3a illustrates the measurement setup that is used to study the touch-induced performance of the RFID tag. We attach a single RFID tag that is $1.5 \times 10cm$ in size (shown in Fig. 3b) on a flat surface, and place a $9dBi$ circularly polarized RFID antenna $50cm$ directly below it. The antenna is powered by an Impinj R420 RFID reader. The camera in Fig. 3a only used in later sections for accuracy measurements. For clarity, we divide the tag into 9 equal subsections, as shown in Fig. 3b. Position 5 corresponds to the middle, while 1 and 9 are at the two ends of the tag.

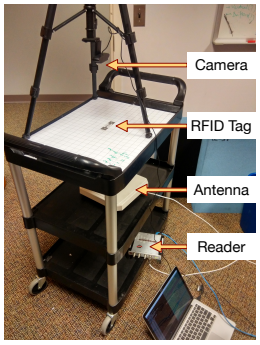

(a) Equipment setup.

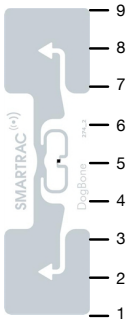

(b) Monza R6 Dogbone RFID tag.

Figure 3: Equipment and tags used in the swipe experiment.

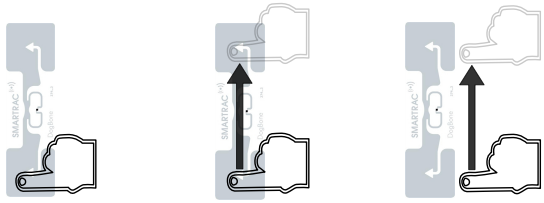

(a) Simple touch. **(b) Swipe on surface.** **(c) Swipe along edge.**

Figure 4: Touch gestures.

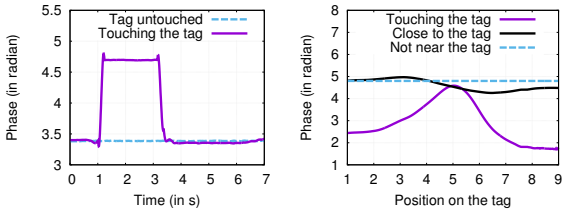

(a) Simple touch at 1 to 3 sec. **(b) Swipe gesture.**

Figure 5: Phase of backscattered RFID signals.

We perform three gestures, as illustrated in Fig. 4: a simple touch gesture where we touch one end of the tag (Fig. 4a), a swipe gesture where we start with a finger on one end of the RFID tag and move across the length of the tag at constant speed (Fig. 4b), and a swipe gesture that is performed along the edge of the tag but without touching the tag itself (Fig. 4c). The RFID reader continuously queries the RFID tag during the entire swipe gesture at a rate of ~200 reads/second. We use the Octane SDK [24] together with the Impinj R420 reader to obtain the phase and magnitude of the backscattered responses from the RFID tag. We make four observations from our experiments:

(1) Human touch induces significant phase changes in the backscattered response. Fig 5a shows the backscattered phase of the RFID tag when a simple touch is applied from 1 to 3 seconds after the start of the experiment. Observe that during this time interval, the backscattered phase jumps from 3.5 to 4.8 radians. The signal phase returns to 3.5 radians once the touch is removed. This demonstrates that a simple touch will induce a significant phase

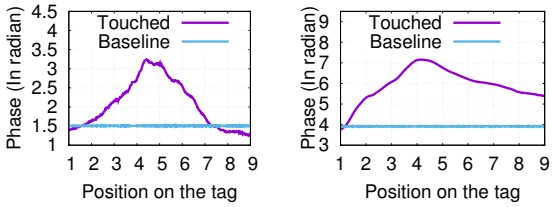

(a) Tag behind a wall. (b) Tag behind door.

Figure 6: Phase-change pattern of backscatter signals with tag in NLOS locations.

change (1.3 radians in this experiment), and is a simple method to detect a touch gesture on an RFID tag. This amount of phase change varies between tags, and can either increase or decrease in response to human touch.

(2) A swipe gesture induces different phase changes as the finger moves over the tag. Fig. 5b shows the absolute backscattered phase under the two different swipe gestures. Observe that with the swipe gesture over the RFID tag, the amount that the phase changes compared to an untouched tag varies depending on the position of the finger. This phase trend follows a symmetrical bell-shape, with about 3 radians between the highest and lowest phases, and starting from one end of the tag, the largest phase-change is seen when the swipe crosses its middle.

(3) Human touch is the dominant cause of phase changes. Fig. 5b also shows the phase of the backscattered signal when the swipe gesture is performed without touching the antenna on the tag. Observe that *while some phase changes are present, they are much less significant than when the touch gesture is performed directly on the tag.* This observation, together with the measurement under NLOS conditions, shows that the dominant effect due to human touch can be measured under varying channel conditions.

(4) Phase behavior is resilient to multipath. In order to study the effect of non-line-of-sight (NLOS), we repeat the swiping gesture but with the tag and reader in different positions by separating them with (a) a wall, and (b) a door. The reader and tag are $2m$ apart. Under such conditions, the indirect signal paths and associated multi-path distortion has a greater impact on the backscatter signal. Note that the maximum range at which an RFID tag can be read depends on both the RFID reader and the tag. Our Monza R6 tags have a theoretical maximum read range of over $6m$, but practically, this limit is close to the $2m$ used in our NLOS experiment.

Fig. 6 shows the phase of the backscattered signal under these two conditions (labeled *Touched*). The *baseline* plot shows the RF phase of the RFID tag without any human contact. Observe that *even in NLOS situations, the bell-shaped phase change behavior seen earlier is maintained.* Hence, even though multipath and NLOS effects can influence the RF phase readings, the impact of human touch on the phase of the backscattered signal is dominant.

3.2 Why Does the Backscatter Phase Change with Human Touch?

The human body can be modeled as an electrical circuit with an equivalent resistance and capacitance [26]. In particular, the human skin has a capacitance equivalent to hundreds of picofarads

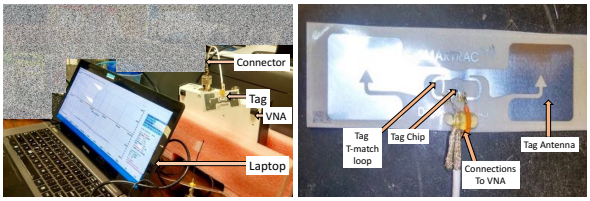

(a) VNA experimental setup. (b) Customized Dogbone RFID tag for VNA experiment.

Figure 7: Vector Network Analyzer (VNA) measurement.

(pF) [14]. When a human touch is established with the RFID antenna, *capacitive coupling* [27] is established between the human and the RFID antenna at the point of contact. We explain the impact of this coupling and verify its influence on the backscatter phase through real-world VNA circuit measurements.

3.2.1 ***Capacitive Coupling.*** The radiation of RF signals from the RFID tag antenna is the result of time-varying current induced within the antenna. A change in the phase of this current will induce a corresponding phase change in the associated RF radiation [28, 29]. Hence, in order to understand how the phase of the backscattered signal changes, it is helpful to know how the phase of this induced current is affected by touch. The RFID tag in our experiments uses a *dipole antenna* [30] for backscatter communications. Using a simplified model of dipole antennas, the current induced in the RFID antenna can be mathematically expressed as [29]

$$I_m = -\frac{E_{\text{inc}}}{(Z_C + Z_A)\gamma \cos^2(\gamma L/4)} \tag{1}$$

where Z_C and Z_A are the impedances of the RFID chip and antenna, respectively, E_{inc} is the incident electric field on the RFID antenna, L is the length of the antenna, and γ is the free-space phase constant. If the effective impedance of the antenna Z_A is changed, (1) shows that the induced current, and by extension, the backscattered electric field and signal, will undergo a corresponding change in phase and magnitude [30]. However, *how does human touch change the antenna impedance?*

Through capacitive coupling, the human body becomes an extension of the RFID antenna. The effective impedance of the RFID antenna, Z_A, as presented to the RFID chip, is now a sum of the impedance of the antenna without human touch and the impedance introduced by the human finger. A change in phase in this effective impedance will cause a corresponding phase change in the current distribution within the antenna. As a result, the phase of the backscattered signal changes in response to human touch.

3.2.2 ***VNA Measurements.*** We directly measure this the impedance change due to human touch using an Array Solutions Vector Network Analyzer (VNA) [31]. We use the same RFID tag from Fig. 3b, but disconnect the RFID chip from the antenna, and solder the feed points of the RFID antenna directly to the electrical leads of the VNA. Fig. 7b shows the modified tag used for our VNA measurements. Using this setup, we can induce electrical currents within the RFID antenna, and directly measure the impedance in the antenna.

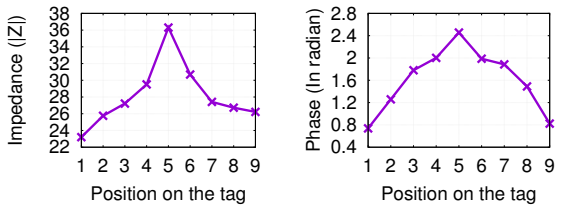

(a) Magnitude. (b) Phase.

Figure 8: Tag impedance change due to human touch.

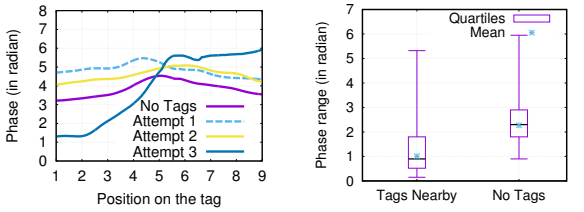

(a) Mutual coupling distorts swipe phase behavior. **(b) Mutual coupling reduces dynamic range of phase change.**

Figure 9: Phase behavior with or without nearby tags.

We again divide the tag into 9 equal subsections, and measure the impedance of the antenna when human touch is applied to each of the 9 points. Fig. 8 shows the magnitude and phase of this measured impedance. Observe that the impedance change also follows a symmetric bell-shaped pattern, with the largest magnitude and phase changes occurring when the human touches the middle of the tag.

3.3 Human Touch on a Multi-Tag Array

Mutual coupling between one or more RFID tags in close proximity can distort the phase and magnitude of the backscattered signal during a swipe gesture [16, 32]. For example, Fig. 9a shows the phase trends of four swipe events over a single RFID tag when (a) there are no other tags in close proximity, and (b) three examples when there is one other tag placed 5*mm* away from it.

Observe that due to mutual coupling, the phase can even be almost invariant at several tag locations when one other tag is adjacent (e.g. positions 6 to 9 in Fig.9a for "w/ adj tag 3"). In the other two swipes with adjacent tags, the dynamic ranges of phase changes reduce to around 0.9 radian. This is equivalent to a reduction in the signal-to-noise ratio (SNR) of the phase data obtained by the RFID reader. Furthermore, Fig. 9b illustrates that dynamic range of phase change in both halves of the curve for mutual coupling scenarios is on an average 1 radian less than the case when no tag is nearby. This poses a challenge for Rio as a low SNR phase data is correlated with worse finger tracking accuracy.

To overcome this challenge, we now try to understand how mutual coupling between tags affects our primitive.

3.3.1 ***Inverted Phase Behavior.*** Our experiments show that due to mutual coupling, when human touch is applied to a tag,

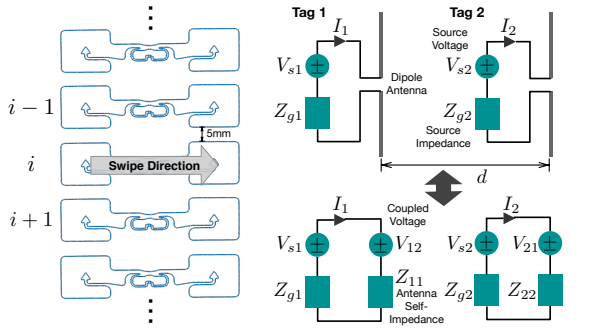

Figure 10: Tag array for coupling measurement.

Figure 11: Equivalent circuit of tags 1 and 2.

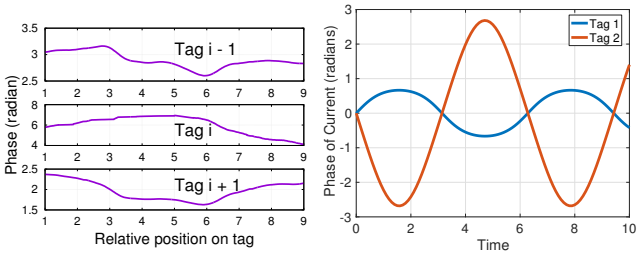

Figure 12: Phase change trends in tags $i-1$ and $i+1$ are the inverse of tag i.

Figure 13: Phase of induced current in tags 1 and 2.

the *trend* of its own phase change is the *opposite* of those seen in adjacent tags.

Fig. 10 shows the tag layout used in this experiment, with each pair of adjacent tags separated by 5*mm*. To highlight the effect of mutual coupling, we consider only three tags in this array, labeled $i-1$, i and $i+1$. We swipe across tag i and record the phase of tags $i-1$, i and $i+1$.

Fig. 12 shows the phase of the backscatter signal measured from these three tags. Observe that due to mutual coupling, tag i experiences a smaller range (around 2 radian lesser) of phase variations during the swipe gesture. However, the trend of the phase changes show an interesting pattern: observe that as the swipe gesture moves across tag i, a increase in its phase coincides with a decrease in the phase of tags $i-1$ and $i+1$. We refer to this phenomenon as the *inverted phase behavior of adjacent tags*. The impact of such mutual coupling diminishes as we consider tags that are farther away than the adjacent tags.

3.3.2 ***Why is the trend of phase changes in adjacent tags inverted?*** **Model:** To understand the impact of mutual coupling on tag interaction, we model the basic scenario of coupling between two tags. The equivalent circuit of the two tags can be represented as shown in Fig. 11. Here, V_{s1} and V_{s2} are the equivalent source voltages induced by the reader's signal on the tag antenna, with Z_{s1} and Z_{s2} being the corresponding chip impedances, and Z_{11} and Z_{22} being their respective antenna self-impedances.

The current in tag 1, I_1 induces a magnetic field, which couples tag 1 and tag 2, thereby inducing a coupled voltage in tag 2, V_{21}, where $V_{21} = I_1 Z_{21}$, and Z_{21} is the mutual impedance in tag 2 due to

tag 1. Similarly, we have the coupled voltage in tag 1 as $V_{12} = I_2 Z_{12}$. Now, taking mutual coupling into account, the resulting voltages, for tag 1 and tag 2 respectively, can be written as,

$$\begin{aligned} I_1(Z_{11} + Z_{s1}) &= V_{s1} + I_2 Z_{12} \\ I_2(Z_{22} + Z_{s2}) &= V_{s2} + I_1 Z_{21} \end{aligned} \tag{2}$$

When a tag is interrogated, the back-scattered field (signal) from a tag is a function of the current in the tag. Hence, it suffices for the analysis to focus on the currents in the two tags to understand how interacting with one tag changes the current in the mutually coupled tag. Solving for the two currents in Equation 2, we get,

$$I_1 = \frac{V_{s1}\tilde{Z}_{22} + V_{s2}Z_{12}}{\tilde{Z}_{11}\tilde{Z}_{22} - Z_{12}Z_{21}};\ I_2 = \frac{V_{s2}\tilde{Z}_{11} + V_{s1}Z_{21}}{\tilde{Z}_{11}\tilde{Z}_{22} - Z_{12}Z_{21}} \tag{3}$$

where $\tilde{Z}_{11} = Z_{s1} + Z_{11}$ and $\tilde{Z}_{22} = Z_{s2} + Z_{22}$.

Phase Change during Tag Interaction: Note that we are interested in modeling the *change in phase* of the signal received by the reader when a user is interacting with the tag being interrogated or a nearby tag. When a tag is interrogated, the signal received by the reader is a combination of the backscattered signal from the desired tag as well as the scattered signal from the other tags (which serve as simple scatterers). We will assume that the contribution of the scattered signals is negligible relative to that of mutual coupling from nearby tags. In this case, the phase of the received signal can be estimated from the phase of the current of the backscattered signal, while accounting for mutual coupling with nearby tags. The phase of the currents in the two tags, I_1 and I_2, can be written as,

$$\angle I_1 = \phi_1 - \phi_m, \text{ and } \angle I_2 = \phi_2 - \phi_m \tag{4}$$

where ϕ_1, ϕ_2 and ϕ_m are the phases of $(V_{s1}\tilde{Z}_{22} + V_{s2}Z_{12})$, $(V_{s2}\tilde{Z}_{11} + V_{s1}Z_{21})$, and $(\tilde{Z}_{11}\tilde{Z}_{22} - Z_{12}Z_{21})$ respectively.

Now, let us consider the case when the user interacts (touching or swiping) with tag 2. This will change the self impedance of Z_{22} as well as its coupled impedance Z_{12} on tag 1, while the chip impedances Z_{s1}, Z_{s2} and tag 1's self (Z_{11}) and induced (Z_{21}) impedances will not change. Hence, while phases ϕ_1 and ϕ_m will change, ϕ_2 will remain constant. The phase-change behavior can now be captured as,

$$\begin{aligned} \angle I_1(t) &= \phi_1(t) - \phi_m(t) \\ \angle I_2(t) &= \phi_2 - \phi_m(t) \\ \text{where, } \phi_1(t) &= \angle(V_{s1}Z_{s2} + V_{s1}Z_{22}(t) + V_{s2}Z_{12}(t)) \\ \phi_m(t) &= \angle\left(\tilde{Z}_{11}Z_{s2} + \tilde{Z}_{11}Z_{22}(t) - Z_{21}Z_{12}(t)\right) \end{aligned}$$

From the above equation, it can be observed that $\phi_1(t)$ and $\phi_m(t)$ are essentially functions of the same impedance changes, namely $Z_{22}(t)$ and $Z_{12}(t)$. However, the change in $Z_{12}(t)$ has an opposite effect in $\phi_1(t)$ compared to that in $\phi_m(t)$. This contributes to a counter-acting effect on the phase change of $I_1(t)$ compared to $I_2(t)$ (i.e. tag being touched), and results in the inverted phase-change behavior between the tags. To highlight this impact, we plot the phase evolution of $I_1(t)$ and $I_2(t)$ in Fig. 13. Here, $Z_{22}(t)$ is assumed to vary as a sine function during human interaction (for illustration), while $Z_{12}(t)$ is assumed to vary proportionally to $Z_{22}(t)$ (in both magnitude and phase), and rest of the non-varying complex quantities are assumed to be real with unit magnitude.

Thus, while leveraging the primitive for tracking could lead to reduced accuracy in the presence of mutual coupling, the above measurements and analysis highlight the predictable impact of mutual coupling on our primitive. Hence, by leveraging the phase-change behavior across neighboring tags jointly, our primitive can be made robust to mutual coupling in multi-tag settings.

4 RIO DESIGN

Leveraging the above characteristics of the primitive, we now design the algorithms needed to track the path of the human finger during a swipe gesture across a single isolated tag, and across any individual tag within a tag array. Note that for the sake of simplicity, Rio only tracks a continuous, one-direction swipe across a tag starting from location 1 and ending at 9, as shown in Fig. 4b. This is not a fundamental limitation of Rio, and the algorithms can be extended to support arbitrary touch movement within a tag.

4.1 Finger Tracking on a Single RFID Tag

Single-tag swipe tracking is done in two stages. Rio first detects a touch event on the tag. Once a touch is detected, Rio uses an online tracking algorithm, Rio-Single, to track the position of a human finger across the single tag. A simple, low-overhead calibration is first performed on a tag that is attached to a surface to determine the precise characteristics of the bell-shaped phase trend. This calibration overhead is small and needs to be performed only once after the tag is first installed. Rio then uses a tracking algorithm based on *segmental dynamic time warping (SDTW)* [33–35] that allows for good tracking accuracy with only limited calibration overhead.

4.1.1 ***Low-Overhead Tag Calibration.*** Tag calibration has to be conducted once after the tag is installed on a surface. During tag calibration, the user swipes his/her finger across the surface of the RFID tag at constant speed (as constant as possible), while the Impinj R420 RFID reader continuously reads the tag at a rate of 200 reads/second, and records the phases of all backscatter responses. Rio *normalizes* the phase responses w.r.t. the lowest value:

$$p(x) = r(x) - \min_x r(x), \quad 0 \le x \le L \tag{5}$$

where $r(x)$ is the unnormalized (i.e. raw) phase values at location x from the calibration swipe across a tag of length L. Rio then uses polynomial curve-fitting to find the fourth-order polynomial that best describes the normalized calibration data.

Overhead. This calibration is repeated four (4) times. Rio uses the average of the four polynomial curves in the next touch detection/tracking step. This low-overhead calibration step is (a) *not* user-specific, and (b) only specific to the installed location of the tag. Hence, each installed tag only needs to be calibrated once before touch tracking is enabled for all users thereafter. Due to human limits, it is not possible to replicate a swipe with a human finger precisely. We have empirically determined that the average of four swipes is sufficient to capture the key behavior of an actual human swipe. We have validated this by having one person calibrate the tag, and evaluating the tracking accuracy of Rio with fifteen (15) other human individuals. Our tracking error remains under 4% for all the sixteen (16) individuals. Note that, we do not need to re-calibrate Rio if only the reading angle of the antenna or the tag

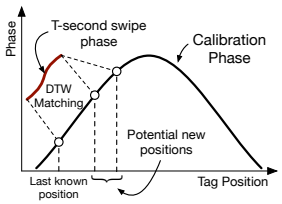

Figure 14: DTW search is applied to each window of samples during a swipe.

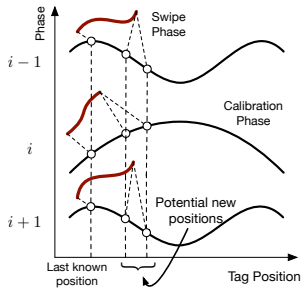

Figure 15: DTW search across adjacent tags.

changes. However, if there is some considerable change in the environment (e.g., introduction of more blockage due to new furnitures or more dynamic paths due to increased movements of people), we need to recalibrate to create the basic phase trend to achieve accurate tracking.

4.1.2 ***Rio-Single Algorithm.*** Rio uses a two stage approach to finger tracking. Rio continuously reads the RFID tag until it detects a touch event. Once a touch has been detected, Rio switches to a tracking stage where it tracks the position of the finger as it is swiped across the RFID tag.

Touch Detection. A touch event results in a significant change in the phase of the response signal from the tag. Rio queries the tag continuously and finds the average signal phase over every time interval of T seconds. If a significant change is seen from one time interval to the next (a change larger than a threshold C), then a touch event has occured and Rio switches to a tracking mode. Rio uses a threshold of $C = 0.9$ radians, which is empirically determined to provide 100% detection accuracy in real-world conditions.

Touch Tracking. Rio updates the location of the finger during a swipe gestures using a segmental dynamic time warping (SDTW) search algorithm. A good overview of SDTW can be found in [35]. Broadly speaking, SDTW compares two sequence segments by stretching and squeezing (*i.e.*, warping) one of the sequences until an optimal match between them is found. The measure of similarity of between these two sequences at this optimal match is returned by the SDTW algorithm.

Fig. 14 illustrates how Rio updates the estimated location of the finger in real-time. Rio first collects a sequence of phases of all backscatter responses over a time window of T seconds. Starting from the previously estimated position of the finger, Rio begins a DTW matching by warping the collected sequence and comparing it against multiple *segments* of the calibration phase data. These segments start from the last known position of the finger, and have varying lengths that span the range of potential new positions, as shown in Fig. 14. The segment with the best match is chosen, and its corresponding end position is taken as the new position of the finger.

This search-and-update step is continuously repeated as Rio tracks the finger over the surface of the tag. The details of the touch detection and tracking algorithms are described in Algorithm 1.

Rio estimates the finger location after every time interval T seconds. The choice of T determines the latency and processing overhead of each location estimate. In our implementation of Rio, we use $T = 0.5s$ as we have empirically determined it to be suitable for a typical swiping speed. We have evaluated the performance of Rio for other values of T and found the performance to be similar.

Algorithm 1 Rio-Single

```
1:  x_0 ← current finger location;
2:  x_max ← max finger location w.r.t. x_0;
3:  x_min ← min finger location w.r.t. x_0;
4:  p(x) ← calibration data (from Eq. (5));
5:  procedure DTW(a, b)
6:      return DTW distance between sequences a and b;
7:  procedure minDTW(x_0, x_1, w, p(x))
8:      p ← {p(x)|x_0 ≤ x ≤ x_1}; ▷ Segment of calibration phase data between x_0 and x_1
9:      return DTW(w, p − p(x_0));
10: procedure getPhaseData
11:     t_0 ← currentSystemTime;
12:     t ← t_0; w ← emptyVector;
13:     while t ≤ t_0 + T do
14:         t ← currentSystemTime;
15:         w ← append(w, currentPhaseReading);
16:     return w − min(w);
17: procedure updateLocation(x_0, w)
18:     x_new ← arg min_{x_min<x<x_max} minDTW(x_0, x, w);
19:     return x_new;
20: procedure touchDetection
21:     while True do
22:         w ←getPhaseData;
23:         if mean(w) > C then return True;
24: procedure touchTracking
25:     while True do
26:         w ←getPhaseData;
27:         x_0 ← updateLocation(x_0, w);
28: touchDetection(); touchTracking();
```

In Algorithm 1, Rio performs a DTW search over a range of segment sizes, as specified by $x_{\min}$ and $x_{\max}$ in Algorithm 1. $x_{\min}$ and $x_{\max}$ determine the lower and upper ranges of swipe gesture speeds that will be accurately tracked by Rio. The greater the value of $x_{\max}$ the higher the upper bound of this speed limit. Similarly, the smaller the value of $x_{\min}$, the slower the lower bound on the speed limit. We select $x_{\min}$ and $x_{\max}$ to correspond to $0.5T$ and $1.5T$ seconds of calibration data respectively, which is equivalent to a swiping speed of 10 to $15mm/s$.

4.1.3 ***Computation Overhead.*** The computational overhead of finger tracking is dominated by the the DTW algorithm, which has a complexity of $O(N^2)$. In practice, Rio samples M equally spaced sample sizes from the range of $x_{\min}$ and $x_{\max}$, and performs a location update (procedure updateLocation in Algorithm 1) over these M samples. The larger the number of samples M, the finer the tracking resolution. However, the overhead of the corresponding search will also be significantly greater. By default, Rio uses $M = 200$ to achieve high accuracy. However, our empirical evaluations, as shown in Fig. 24, show that we can reduce M to 50 with only a slight reduction in accuracy, but gain a 4× reduction in computation delay. With $M = 50$, each full tracking update step can be accomplished in under a second, thus enabling real-time tracking of the finger position. Hence, an interface that is built with Rio can tune M to match the desired accuracy-overhead trade-off.

4.2 Finger Tracking on a Multi Tag Array

We consider the tag array layout as illustrated in Fig. 10. Rio tracks a finger on a multi-RFID tag array with two steps. Rio first identifies the tag that the finger is touching, while accounting for mutual coupling. Once Rio determines the tag that is touched, it uses a multi-tag tracking algorithm (using neighboring tags) to continuously localize the finger during the swipe gesture.

4.2.1 ***Tag Calibration.*** As in the single tag case of §4.1.1, calibration has to be performed on the tag array only once after installation. Rio collects and normalizes the phases as the user swipes his/her finger across each tag in the array, as shown in Fig. 10. We use $p_1(x), \ldots, p_N(x)$ to refer to the normalized phases from the N tags in the array.

Algorithm 2 Rio-Multi: Touch Detection

```
1:  procedure phaseDiff(w)
2:      s ← linearRegression(w)
3:      return max{s} − min{s}
4:  procedure touchDetect(w_1, ..., w_N, L)
5:      for i = 1, ..., N do
6:          d_i ← phaseDiff(w_i)
7:      for i = 1, ..., N do
8:          if i = 1 then
9:              m_i ← αd_i − βd_{i+1}
10:         else if i = N then
11:             m_i ← αd_i − βd_{i−1}
12:         else
13:             m_i ← αd_i − β(d_{i−1} + d_{i+1})
14:     i^(1) ← arg max_{i∈{1,...,N}} m_i
15:     return i^(1)
```

4.2.2 ***Rio-Multi Algorithm.*** **Touch Detection.** Touch detection operates on the backscatter phase from all N tags over a time window T. We use $\mathbf{w}_1, \ldots, \mathbf{w}_N$ to refer to these N vectors of phase data. Informally, Rio determines the total change in phase encountered by each tag over this time window. It then searches for the tag triple (or tag pair, in the case of the tags at either ends of the array) that best demonstrates the *inverted phase behavior* as described in §3.3: for a given tag i, the change in phase of its neighboring tags $i-1$ and $i+1$ are the inverse of its own.

Algorithm 2 shows the pseudo-code for touch detection. The phaseDiff procedure determines the phase changes over the window of phase data. Rio smooths out the noise in the phase data by fitting the best line through the phase data using linear regression. The phase change of each tag, d_i, is the difference between the two extreme points on the line. Rio computes a weighted sum of the phase change of each tag i and its neighboring tags as $m_i = \alpha d_i - \beta(d_{i-1} + d_{i+1})$. By selecting weights α and β with opposite polarity, Rio can capture the effect of the inverse phase behavior of tag triples (or tag pairs). Empirically, we have found that the touch and tracking accuracy of Rio is best when $\alpha = 0.8$ and $\beta = 0.2$.

Touch Tracking. Once Rio has determined the specific tag that is being touched, it immediately begins reading phase data from that tag i, along with tags that are directly adjacent to it, tags $i-1$ and $i+1$ (if any). Fig. 15 illustrates how the segmental DTW search is extended to support two adjacent RFID tags. Rio conducts concurrent DTW searches on these three tags (or two tags, if i is an edge tag), using the same segment sizes for each step in the DTW search. The segment size that best matches the phase data from the three tags will indicate the new finger location.

Algorithm 3 Rio-Multi: Touch Tracking

```
1:  x_0 ← 0                                              ▷ Current finger location
2:  w_1, ..., w_N ← getAllPhaseData
3:  i_max ← touchDetect(w_1, ..., w_N, L)
4:  procedure minMultiDTW(x_0, x, w_{i−1}, w_i, w_{i+1})
5:      g_i ← minDTW(x_0, x, w_i, p_i)
6:      g_{i−1} ← minDTW(x_0, x, w_{i−1}, p_{i−1})
7:      g_{i+1} ← minDTW(x_0, x, w_{i+1}, p_{i+1})
8:      h ← αg_i + β(g_{i−1} + g_{i+1})
9:      return h
10: procedure updateLocation(x_0, w_{i−1}, w_i, w_{i+1})
11:     x_new ← arg min_{x_min≤x≤x_max} minMultiDTW(x_0, x, w_{i−1}, w_i, w_{i+1})
12:     return x_new
13: while True do
14:     x_0 ← updateLocation(x_0, w_{i_max−1}, w_{i_max}, w_{i_max+1})
15:     w_{i_max} ←getPhaseData
16:     w_{i_max−1} ←getPhaseData
17:     w_{i_max+1} ←getPhaseData
```

Algorithm 3 shows the multi-tag tracking algorithm. The minMultiDTW procedure performs the multi-tag DTW search jointly on sets of three adjacent tags and combines the results using the weighted metric $h = \alpha g_i + \beta(g_{i-1} + g_{i+1})$ where g_i, g_{i+1} and g_{i-1} is the DTW distance of tag i, $i-1$ and $i+1$ respectively. This metric identifies segments that not only match the phase pattern in the desired tag but also the inverted phase pattern in the adjacent tags, to boost the tracking accuracy. The segment identified in the updateLocation procedure is used to update the new location of the finger during the swipe. As before, Rio runs this search-and-update procedure continuously to track the location of the finger.

4.2.3 ***Scaling to Larger Multi-Tag Arrays.*** RFID readers achieve a constant number of reads/second (200 in case of our Impinj reader), regardless of the number of tags within the read range. Hence, when the array size is very large, the read rate per tag decreases, which reduces the fidelity of the phase data, and consequently the accuracy of both touch and gesture tracking. Rio addresses this by utilizing the PHY-layer filtering feature [36] of the RFID Class 1 Generation 2 (C1G2) protocol to read only subsections of the array at a time. After Rio-Multi detects the tag that is being touched, Rio applies the RFID filter to read up to eight tags around the tag that is touched (four on either side). The Rio-Multi touch tracking then tracks the swipe gesture on the touched tag.

5 EXTENDING RIO WITH CUSTOM DESIGNED RFID TAGS

COTS RFID tags are designed primarily for communications, and hence, the antennas are typically dipole antennas, and have sizes and shapes that are carefully tuned to match the electrical impedance of the RFID chip [21]. The limited variety in antenna designs restricts the range of user interfaces that can be built using COTS tags. In this section, we discuss Rio's potential by exploring how it can operate with custom-built RFID tags of varying shapes and sizes. This will allow the user interfaces built using our touch primitive to be better customized to the specific demands of smart spaces.

Constructing Custom RFID Tags. We extend Rio to support custom-designed RFID tags, two of which are shown in Fig. 16.

(a) Circle custom tag. (b) Triangle custom tag.

Figure 16: Custom-designed RFID tags.

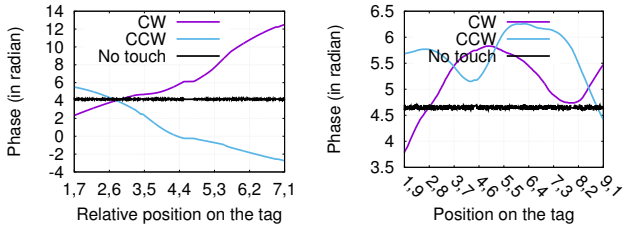

(a) Circle tag. (b) Triangle tag.

Figure 17: Phase trends when a clockwise (CW) and counter-clockwise (CCW) swipe gestures are performed on the custom circle and triangle-shaped RFID tags.

The antenna of the tags are constructed using copper metal tape, arranged in shapes that can better mimic familiar control interfaces. For example, Fig. 16a shows a circle RFID antenna that resembles a round control knob. A user can swipe in either clockwise or counter-clockwise directions to adjust the music volume, or light brightness etc. Owners of the iPod Classic with the click wheel [37] will find this interface familiar. A small near-field RFID tag [38] with an adhesive side is attached to the custom-built antenna, as shown. The antenna forms an inductively coupled connection with the near-field RFID tag, and touching the antenna will result in a familiar phase change in the backscattered signal.

Antenna Design Space. The antennas shown in Fig. 16 are examples of *loop antennas* [39]. We use loop antennas because they have the advantage of being easy to construct in various shapes and sizes. Our demonstration only uses basic shapes (a circle and a triangle), but many other antenna structures such as folded dipoles [40], coil [41] and cloverleafs [42] can be used as building blocks for more complex interfaces.

In order for the antenna to operate at maximum efficiency, the antenna layout must be tuned such that its impedance matches the impedance of the RFID chip. Our custom RFID antennas are designed primarily to mimic real-world control interfaces, and are not impedance-matched to the RFID chip. However, even with this sub-optimality, our experiments show that our custom tags can be read at ranges of up to 1.5m, which is comparable to the performance of COTS RFID tags 2.4m.

Tracking on Custom Tags. Fig. 17 shows the phase trends when clock-wise and counter-clockwise swipes are performed on the tags (Fig. 16). Observe that the phase trends show distinctive patterns and large phase variations (similar to those seen in COTS RFID tags) that can aid in accurately locating a finger even in the presence of noise. Thus, the single tag tracking algorithm (Algorithm 1) in Rio can also be used to track touch/gesture with these custom tags.

6 RIO EVALUATION

In this section, we evaluate Rio using the setup shown in Fig. 3a. We show the performance of Rio with COTS tags, as well as custom-designed tags and highlight its robustness as a battery-free UI primitive. We also propose and evaluate two proof-of-concept applications to demonstrate the utility of Rio.

The RFID setup operates as before, where the Impinj R420 reader continuously queries the tags in range (at ~200 reads/second), and records the RF phase of all RFID responses. We thus have time series of phase readings for each individual tag. The camera is time synchronized with the reader control software, so that the video recording is time synchronized with the RF phase measurements. This video footage is used to determine the tracking accuracy.

COTS Tag Layout. We demonstrate the swipe tracking accuracy of Rio using the COTS tags. We use two different tag layouts: a single isolated tag, and a multi-tag array, as shown in Fig. 10. This tag layout has two parameters: Tag angle, and distance. *Tag angle:* Fig. 3a shows a setup where the tags are place flat on a surface, which is parallel to the plane of the RFID reader antenna. We tilt the reader antenna by elevating one edge of the antenna to vary the angle of the tag(s) w.r.t. the reader antenna. *Tag distance:* We also elevate the entire tag(s) shown in Fig. 3a to vary the distance of the tags to the reader antenna. Experiment result with different tag angle and distance serve to demonstrate the performance of Rio under real-world conditions, when the tag is not perfectly aligned with the antenna.

Custom Tags. We also evaluate Rio on custom tags, as described in §5. These custom tags are arranged 50cm away from, and parallel to the surface of the reader antenna.

Accuracy Measure. We use OpenCV [43] on the time-synchronized video footage to visually track the finger during the swipe and touch gestures. At any point in time, we compare the location of the finger as indicated by Rio to its actual finger position as shown by the camera. The tracking accuracy of Rio is reflected in the offset distance (in mm) between these two measurements (Rio and camera).

6.1 RIO with COTS Tags

6.1.1 ***Touch Detection.*** **COTS Single Tag.** For single-tag detection, we use the phase change threshold $C = 0.9$ as described in §4.1.2. With this threshold, Rio achieves perfect touch detection, even under varying tag angles (from 0 to 60°, w.r.t. the reader antenna surface) and tag distances (up to 2.4m from the reader).

COTS Multi-Tag Array. Fig. 20 shows the detection accuracy when we touch each tag in an array of eight tags. Observe that Rio correctly detects the tag being touched more than 92% of the time. Touch events on tags closer to either ends of the array are even correctly detected 100% of the time. Hence, *Rio provides close to perfect tag detection under real-world conditions, with RFID tags deployed in positions within an envisioned smart space.* We expect this accuracy to increase if multiple receive antennas, together with spatial diversity processing (*i.e.*, a multi-static setup) is used.

6.1.2 ***Touch Tracking.*** **COTS Single Tag.** Fig. 18 shows the tracking accuracy distribution of a swipe gesture when the tags are parallel to and at a distance of 50cm from the reader antenna. The swipe is performed at three different speed ranges: slow (less than 10mm/s), medium (10 to 15mm/s) and fast (quicker than 15mm/s).

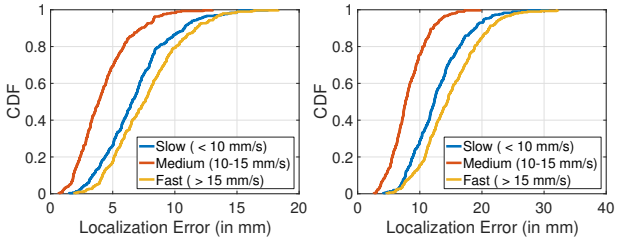

(a) RIO-SINGLE. (b) RIO-MULTI.

Figure 18: RIO tracking accuracy with swipes of different speeds.

(a) Smartrac Monza R5 RFID tag (Tag1). (b) Smartrac Monza R6 G2IL RFID tag (Tag2).

(c) Alien-9640, Higgs-3 short-dipole paper tag (Tag3). (d) Alien-9730, Higgs-4 short-dipole paper tag (Tag4).

Figure 19: RIO is tested on four other tag types.

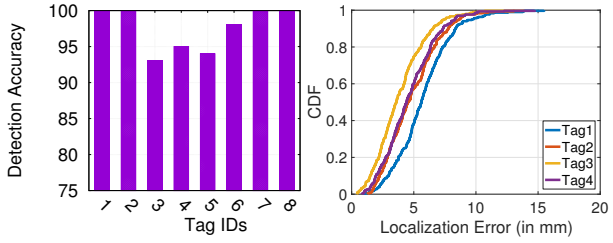

Figure 20: Touch detection on multi-tag array.

Figure 21: Swipe error distribution for 4 other tags(Tag1, Tag2, Tag3, Tag4).

A swipe at each speed range is repeated 100 times on each tag to obtain this distribution. Recall that the DTW window of $0.5T$ to T is chosen for swiping speeds of up to $15mm/s$. Observe that the median location error at medium speed over a single tag, as shown in Fig. 18a, is $3mm$. Given that the tag is $80mm$ in length, this median error is a mere 3.8% of the tag length. The median error with slow and fast swipes is greater, at 7 and $8mm$ respectively, but is still within 10% of the tag length.

This good single tag performance is not limited to our specific RFID tag. To demonstrate this fact, we perform the medium-speed swipe gesture over four other types of tags with different antenna designs and RFID chips, as shown in Fig. 19. Fig. 21 shows that the median tracking error lies between 3 and $6mm$, less than 10% of the tag length.

COTS Multi-Tag Array. Fig. 18b shows the tracking error distribution in an array of eight (8) tags. These results assume perfect touch detection accuracy. Observe that the results show similar behavior to the single-tag case, where the medium speed swipe has this lowest median error of $7mm$, while the slow and fast speeds have median errors of 12 and $14mm$. Hence, even in the presence

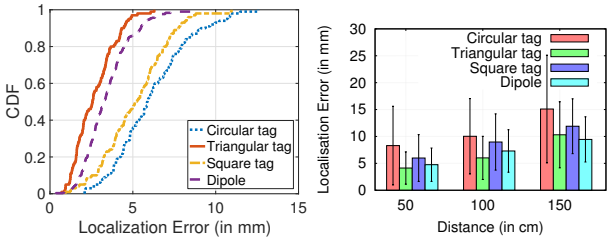

Figure 22: Tracking error distribution of custom tags.

Figure 23: Tracking accuracy of custom tags at different distances from reader.

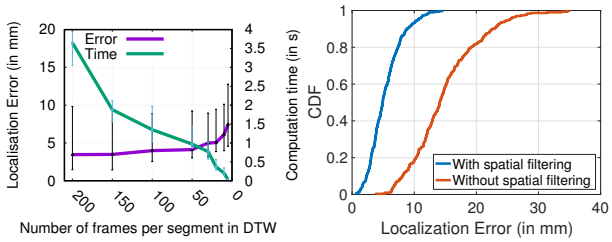

Figure 24: Tracking resolution vs computational overhead.

Figure 25: Swipe tracking accuracy over an array of 30 RFID tags.

of mutual coupling effects, RIO can localize the finger to within 10% of the overall tag length. The experiments on both the single and multi-tag arrays demonstrate that *RIO can accurately track the location of a finger during a swipe gesture.*

6.2 RIO with Custom-Designed Tags

We evaluate RIO with four different types of custom tags: the circle and triangle, as shown earlier in Fig. 16, along with a square and dipole that are constructed with the same techniques. We place the smart tags $50cm$ away from the reader antenna, and perform a medium-speed swipe gesture. Fig. 22 shows the tracking accuracy distribution when a swipe a performed on each of these four custom tags. Observe that the median tracking error of all four tags is less than $8mm$, which is comparable to that obtained using COTS RFID tags. Fig. 23 shows the localization error distribution when the custom tags are placed at distances up to $1.5m$ away from the reader. Observe that even at this distance, the median tracking error is no more than $15mm$, or less than 19% of the tag length. Hence, *RIO readily supports custom designed RFID tags that are purpose built for specific smart spaces.*

6.3 RIO is a Robust Touch-Sensing Primitive

6.3.1 ***Tracking Resolution vs Computation Overhead.*** RIO trades off finger tracking resolution and computational overhead through the number of segments, M, used for each location update (procedure UPDATELOCATION in Algorithm 1) and Algorithm 3. For RIO, we run the data processing and pattern recognition module at an Intel desktop with a 2.93GHz Core i7 CPU and 16GB of memory, running Ubuntu 14.04 and JDK8.

Fig. 24 shows this trade-off for several values of M. Observe that M can be chosen to be as low as 50 with only a slight increase

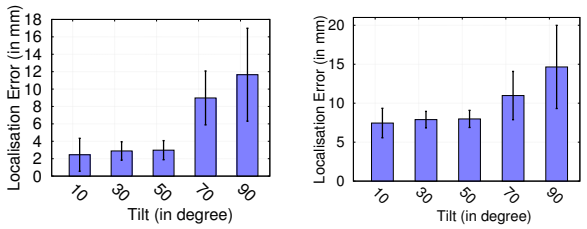

(a) Single tag. (b) Multi-tag array.

Figure 26: Tracking accuracy with varying tilt angle of the tag with respect to antenna.

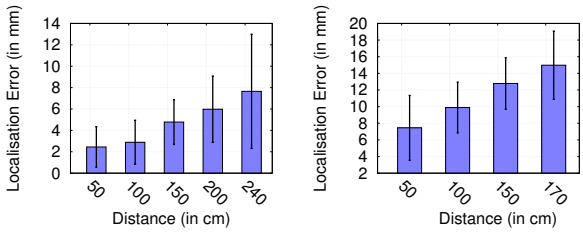

(a) Single tag. (b) Multi-tag array.

Figure 27: Tracking accuracy with varying distance of the tag from the reader antenna.

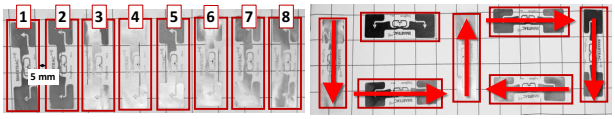

(a) Keyboard with 8 buttons. (b) Numeric touchpad with digit "6" traced (shown rotated 90°).

Figure 28: Example applications.

in median error (from 3 to 4*mm*), while achieving an almost 4× reduction in computation time. At this chosen level of accuracy, RIO has a touch location tracking response time of one second. This computational overhead applies to both single and multi-tag setups. We note that these latencies relates to *motion tracking* only. A simple single-point touch-event can be detected within several milliseconds.

6.3.2 ***RIO on Large Multi-RFID Tag Arrays.*** We evaluate the performance of Rio-Multi with 30 RFID tags, using the same experimental setup as that in §6. Fig 25 shows the tracking accuracy distribution of Rio with and without RFID spatial filtering. Observe that the median tracking error reduces from 14*mm* when no spatial filtering is used, to 6*mm* when filtering is enabled.Due to the large number of tags, when no filtering is used, there are time windows of T seconds when only a small number of phase data is obtained from the tag being touched. This results in poor tracking accuracy. However, no such abnormalities are observed when PHY-layer tag filtering is used.

6.3.3 ***Robust Tracking under Varying Tag Tilt Angles.*** Fig. 26 shows the tracking accuracy of a medium speed swipe when the tags are placed at varying angles w.r.t. the plane of the RFID reader antenna. Observe that in both the single and multi-tag array, Rio can track the finger location with a very small error (at 3 and 8*mm* respectively) when the tag is within 50°, of the reader antenna. This is because the RFID tags have linearly polarized directional antennas that focus the backscatter signals within a 120°, beam-width [44]. This result shows that *battery-free touch or gesture sensing is robust over a large range of incident angles to the RFID reader.* As the tilt angle increases to greater than half the beam-width and the reader antenna moves outside the beam edge of the RFID tag, the tracking accuracy decreases. Note that changing the relative tilt angle of the tag is analogous to the change of the relative angle of the RFID antenna, and will thus yield similar accuracy results.

6.3.4 ***Robust Tracking at Varying Distances from Reader.*** Fig. 27 shows the tracking accuracy when a medium-speed swipe is performed on a tag that is at varying distances from the RFID reader. Observe that in the single tag case, a low error of no more than 8*mm* (10% error) is achievable up to 2*m* from the reader. This demonstrates that *battery-free touch/swipe tracking is robust at varying distances from the reader.* However, if we change multiple factors simultaneously (e.g. reading angle, tag tilt, blockage etc.) or we change one of the impacting factor drastically (e.g. sudden increase of people in the room or introducing a new blockage between the tag and the antenna), we need to re-calibrate RIO to create the reference phase pattern to achieve mm-level accuracy.

6.4 Proof-of-Concept Applications

Rio is a touch sensing primitive for battery-free UI design. In this section, we describe and evaluate two proof-of-concept UI applications that are built using Rio.

Battery-Free Keyboard. A keyboard directly uses the touch-detection capability of RIO in a multi-tag environment. We use Rio to develop an 8-key musical keyboard (as shown in Fig. 28a), along with an accompanying GUI. We can touch multiple keys simultaneously in this musical keyboard application. Fig. 29a shows the false positive (tag is mistakenly detected as being touched) and false negative (a touch event on a tag is missed). Observe that our simple threshold based touch detection algorithm achieves high accuracy in this battery-free key detection system, with a total false positive and negative rates below 10%.

2D Numeric Touchpad. We have constructed a 2D numeric touch-pad, as shown in Fig. 28b, using 7 COTS RFID tags. Each numeric digits is formed by tracing its shape over the RFID tags. Fig. 28b illustrates the outline of the number "6" (shown rotated 90°) traced on the touch-pad.

Fig. 29b shows the accuracy results when numbers 0 to 9 are drawn on this touch-pad. Each number is repeated 50 times, and the false positive and negative rates are reported here. Observe that all individual numbers can be detected with total errors of less than 15%. This shows that RIO with COTS tags can be used to design a general-purpose UI.

7 POINTS OF DISCUSSION

Naturally there is much room for further work and possible improvements. We discuss a few points here.

Cost of Rio system: Rio can support multiple tags simultaneously for single point touch tracking using single antenna and single RFID reader. Currently, this combined unit with one antenna, one RFID reader, costs approximately $1600. We expect that

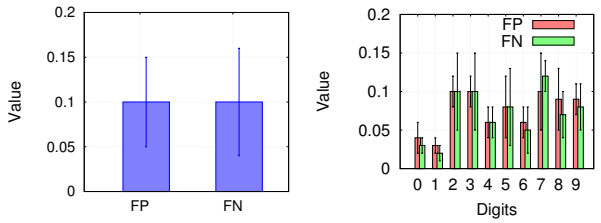

(a) Key press detection. **(b) Numeric digit sensing.**

Figure 29: False positive and negative rates for applications.

dedicated RFID sensing platforms built upon lower-cost hardware (e.g. ThinkMagic reader hardware [45]), together with low-cost off-the-shelf tags will eventually be available to consumers.

Comparison with touch-based sensing: Capacitive touch screens [46] found in smartphones, tablets, laptops and the recently introduced PixelSense [47] offer a readily-available multi-touch interface. However, smart spaces demand low-cost, low-powered, flexible touch interfaces that can be readily integrated into existing off-the-self items. Current capacitive touch screen technology cannot be easily and cost-effectively integrated into our envisioned smart spaces. We note that Rio offers a touch primitive to enable smart spaces and does not replace capacitive touch technology in all applications. Rather, we expect that Rio will integrate with and extend existing capacitive touch interfaces. For example, while Rio detects our direct interactions with the environment, these interactions can be managed through capacitive touch interfaces on our mobile devices.

Multi-touch tracking: Rio is basically a single touch-tracking system and in near future, we plan to extend it to multi-touch tracking interface. This extension will broaden Rio's potential use-cases. However, for this, we have to model more complex mutual coupling phenomenon to provide accurate impedance tracking.

Impact of different blockage scenarios: Although we have shown in Fig. 6 that the phase pattern maintains its shape even in the presence of obstacles like door or wall, the experiments are not exhaustive for different static or dynamic blockage scenarios. In near future, we plan to conduct more experiments in different types of blockage scenarios and different environment conditions to better understand the performance of Rio.

8 RELATED WORK

The core idea of using RFID tag as an input mechanism is not new. Researchers have used either tags with micro-controllers [48] or passive tags in a COTS or custom setup. In the following, we explore main research trends.

RFID-based gesture and activity recognition: RFID tags are used to recognize gestures or activities based on distinct phase and RSS signatures. Researchers [7, 49] have implemented a matrix of RFID tags with multiple antennas to detect gestures. Recently, a few systems [6, 50–52] have used machine learning to mine the phase data for predicting fine-grained exercising or shopping activities. Rio is orthogonal to such works as it targets fine-grained swipe tracking over a smaller area. In fact, Rio can be deployed in conjunction with such activity recognition techniques for a comprehensive IoT environment.

RFID-based fine-grained tracking: Wang *et al.* [10] track tag movement with 8cm median error by using customized 8 antennas. Moreover, *PolarDraw* [53] uses two linearly polarized COTS antennas and exploits polarization property to track a RFID tag. However, *Tagball* [54] employs extended kalman filtering (EKF) [55] technique on collected phase information to create a 3D mouse with 12 tagged object. Furthermore, *Tagyro* [19] exploits phase information of multiple tags to get the orientation of the object with a median error of 4 degrees. Rio is an evolution of such systems into one that enables robust fine-grained tracking on 2D surfaces using only a single antenna.

RFID-based sensing: Marocco *et al.* [56] observes that the change in tag signal RSS and phase due to change in tag antenna performance is related to the change in the environment. This observation underpins RFID tag designs used to measure temperature [57, 58], relative humidity [59–61], and gas presence [62]. Smith *et al.* [63] proposes building switches by connecting ICs with different IDs to the tag antennas. The authors in [12] design a custom backscatter circuit to use the tag antenna as both an RF antenna and a low-frequency capacitance induced electric field sensor simultaneously. This custom circuit enables battery-free detection of singular touch events. Rio is a further development of these works and shows that fine-grained touch and swipe tracking is feasible even with off-the-shelf hardware through the use of our novel impedance tracking techniques.

RFID-based UI: Early works [64, 65] use active tags as power-free buttons. Li *et al.* [8] use a single antenna to enable motion detection in their object interaction detection system called ID-Sense. It uses a Support Vector Machine (SVM) with a Radial Basis Function (RBF) kernel to detect five classes of tag interactions using PHY-layer features (RF Phase, RSSI, read rate, etc.). The SVM is trained using 600 interaction instances and achieves up to 97% accuracy. PaperID [9] is a similar work that uses supervised machine learning to detect 5 types of on-tag and free-air interactions with custom-designed RFID tags. It achieves a 94% accuracy (testing done by 5 users) by using the trained model from 150 instances at different locations. Rio improves upon these works by achieving high accuracy (4% error rate) using off-the-shelf hardware and an extremely low training overhead (only 4 swipe instances required).

9 CONCLUSION AND FUTURE WORK

In this paper, we develop and evaluate Rio, a touch and gesture UI primitive for smart spaces. Rio enables fine-grained touch tracking using COTS RFID reader and tags, and low-overhead training and installation. Rio is designed to be easily embedded into existing environments to turn them into smart spaces. Our evaluations demonstrate that Rio is a robust touch and gesture sensing primitive under various real-world situations. Rio also supports custom-designed RFID tags for a fully integrated UI design and our proof-of-concept applications highlight possible interfaces that can be built with Rio.

Rio is a first step towards a novel battery-free interface design, and presents many opportunities for future exploration into this space. Some extensions of our work that include two-dimensional gesture tracking, multi-touch tracking, tracking in different environment conditions (i.e. rain, snow etc.) and custom interfaces built using different materials. These and more are left to future work.

REFERENCES

[1] Q. Pu, S. Gupta, S. Gollakota, and S. Patel, "Whole-home gesture recognition using wireless signals," in *Proceedings of the 19th Annual International Conference on Mobile Computing & Networking*, MobiCom '13, (New York, NY, USA), pp. 27–38, ACM, 2013.

[2] L. Sun, S. Sen, D. Koutsonikolas, and K.-H. Kim, "Widraw: Enabling hands-free drawing in the air on commodity wifi devices," in *Proceedings of the 21st Annual International Conference on Mobile Computing and Networking*, MobiCom '15, (New York, NY, USA), pp. 77–89, ACM, 2015.

[3] S. Yun, Y.-C. Chen, and L. Qiu, "Turning a mobile device into a mouse in the air," in *Proceedings of the 13th Annual International Conference on Mobile Systems, Applications, and Services*, MobiSys '15, (New York, NY, USA), pp. 15–29, ACM, 2015.

[4] S. Kim, W. Choi, W. Rim, Y. Chun, H. Shim, H. Kwon, J. Kim, I. Kee, S. Kim, S. Lee, and J. Park, "A highly sensitive capacitive touch sensor integrated on a thin-film-encapsulated active-matrix oled for ultrathin displays," *IEEE Transactions on Electron Devices*, vol. 58, pp. 3609–3615, Oct 2011.

[5] M. Kranz, P. Holleis, and A. Schmidt, "Embedded interaction: Interacting with the internet of things," *IEEE Internet Computing*, vol. 14, pp. 46–53, March 2010.

[6] H. Ding, L. Shangguan, Z. Yang, J. Han, Z. Zhou, P. Yang, W. Xi, and J. Zhao, "Femo: A platform for free-weight exercise monitoring with rfids," in *Proceedings of the 13th ACM Conference on Embedded Networked Sensor Systems*, SenSys '15, (New York, NY, USA), pp. 141–154, ACM, 2015.

[7] Y. Zou, J. Xiao, J. Han, K. Wu, Y. Li, and L. M. Ni, "Grfid: A device-free gesture recognition system using cots rfid device," *IEEE Transactions on Mobile Computing*, vol. PP, no. 99, pp. 1–1, 2016.

[8] H. Li, C. Ye, and A. P. Sample, "Idsense: A human object interaction detection system based on passive uhf rfid," in *Proceedings of the 33rd Annual ACM Conference on Human Factors in Computing Systems*, CHI '15, (New York, NY, USA), pp. 2555–2564, ACM, 2015.

[9] H. Li, E. Brockmeyer, E. J. Carter, J. Fromm, S. E. Hudson, S. N. Patel, and A. Sample, "Paperid: A technique for drawing functional battery-free wireless interfaces on paper," in *Proceedings of the 2016 CHI Conference on Human Factors in Computing Systems*, CHI '16, (New York, NY, USA), pp. 5885–5896, ACM, 2016.

[10] J. Wang, D. Vasisht, and D. Katabi, "Rf-idraw: Virtual touch screen in the air using rf signals," in *Proceedings of the 2014 ACM Conference on SIGCOMM*, SIGCOMM '14, (New York, NY, USA), pp. 235–246, ACM, 2014.

[11] L. Yang, Y. Chen, X.-Y. Li, C. Xiao, M. Li, and Y. Liu, "Tagoram: Real-time tracking of mobile rfid tags to high precision using cots devices," in *Proceedings of the 20th Annual International Conference on Mobile Computing and Networking*, MobiCom '14, (New York, NY, USA), pp. 237–248, ACM, 2014.

[12] A. P. Sample, D. J. Yeager, and J. R. Smith, "A capacitive touch interface for passive rfid tags," in *2009 IEEE International Conference on RFID*, pp. 103–109, April 2009.

[13] K. Aga, H. Tarao, and S. Urushihara, "Calculation of human body resistance at power frequency using anatomic numerical human model," *Energy Procedia*, vol. 89, pp. 401 – 407, 2016. CoE on Sustainable Energy System (Thai-Japan), Faculty of Engineering, Rajamangala University of Technology Thanyaburi (RMUTT), Thailand.

[14] N. Jonassen, "Human body capacitance: static or dynamic concept? [esd]," in *Electrical Overstress/ Electrostatic Discharge Symposium Proceedings. 1998 (Cat. No.98TH8347)*, pp. 111–117, Oct 1998.

[15] "Smartrac dogbone rfid paper tag (monza 4d)." https://www.atlasrfidstore.com/smartrac-dogbone-rfid-paper-tag-monza-4d/a, 2017. [Online] Last Accessed : 07/12/2017.

[16] Y. Tanaka, Y. Umeda, O. Takyu, M. Nakayama, and K. Kodama, "Change of read range for uhf passive rfid tags in close proximity," in *2009 IEEE International Conference on RFID*, pp. 338–345, April 2009.

[17] S. E. Asl, M. T. Ghasr, M. Zawodniok, and K. E. Robinson, "Preliminary study of mutual coupling effect on a passive rfid antenna array," in *2013 IEEE International Instrumentation and Measurement Technology Conference (I2MTC)*, pp. 138–141, May 2013.

[18] P. V. Nikitin and K. V. S. Rao, "Theory and measurement of backscattering from rfid tags," *IEEE Antennas and Propagation Magazine*, vol. 48, pp. 212–218, Dec 2006.

[19] T. Wei and X. Zhang, "Gyro in the air: Tracking 3d orientation of batteryless internet-of-things," in *Proceedings of the 22Nd Annual International Conference on Mobile Computing and Networking*, MobiCom '16, (New York, NY, USA), pp. 55–68, ACM, 2016.

[20] K. V. S. Rao, P. V. Nikitin, and S. F. Lam, "Impedance matching concepts in rfid transponder design," in *Proceedings of the Fourth IEEE Workshop on Automatic Identification Advanced Technologies*, AUTOID '05, (Washington, DC, USA), pp. 39–42, IEEE Computer Society, 2005.

[21] P. V. Nikitin, K. V. S. Rao, S. Member, and S. Lazar, "An overview of near field uhf rfid," 2007.

[22] "Impinj speedway uhf rfid reader." https://www.impinj.com/products/readers/, 2017. [Online] Last Accessed : 07/12/2017.

[23] "Epc/rfid llrp standards." http://www.gs1.org/epcrfid/epc-rfid-llrp/1-1-0, 2017. [Online] Last Accessed : 07/12/2017.

[24] "Octane sdk for impinj." https://support.impinj.com/hc/en-us/articles/202755268-Octane-SDK, 2017. [Online] Last Accessed : 07/12/2017.

[25] "Speedway revolution reader application note low level." http://bit.ly/2geiFVA, 2017. [Online] Last Accessed : 07/12/2017.

[26] N. Cho, J. Yoo, S. J. Song, J. Lee, S. Jeon, and H. J. Yoo, "The human body characteristics as a signal transmission medium for intrabody communication," *IEEE Transactions on Microwave Theory and Techniques*, vol. 55, pp. 1080–1086, May 2007.

[27] L. Baxter, *Capacitive Sensors: Design and Applications*. IEEE Press Series on Electronics Technology, John Wiley & Sons, 1996.

[28] R. A. A. Rodrigues, E. C. Gurjão, and F. M. de Assis, "Radar cross-section and electric field analysis of backscattering elements of chipless rfid tag," in *2014 IEEE RFID Technology and Applications Conference (RFID-TA)*, pp. 103–108, Sept 2014.

[29] B. D. Braaten, G. J. Owen, and R. M. Nelson, "Design of space-filling antennas for passive uhf rfid tags," INTECH Open Access Publisher, 2010.

[30] W. Stutzman and G. Thiele, *Antenna Theory and Design*. Antenna Theory and Design, Wiley, 2012.

[31] "Array Solutions VNA-UHF - Two Port Vector Network Analyzer, 5 kHz to 1200 MHz." https://www.arraysolutions.com/vna-uhf, 2017. [Online] Last Accessed : 07/12/2017.

[32] "Mutual coupling in antenna arrays." https://nus.edu/2o5J8IN, 2017. [Online] Last Accessed : 07/12/2017.

[33] A. Park and J. R. Glass, "Towards unsupervised pattern discovery in speech," in *IEEE Workshop on Automatic Speech Recognition and Understanding*, pp. 53–58, Nov 2005.

[34] Y. Zhang and J. R. Glass, "Unsupervised spoken keyword spotting via segmental dtw on gaussian posteriorgrams.," in *ASRU*, pp. 398–403, IEEE, 2009.

[35] A. S. Park and J. R. Glass, "Unsupervised pattern discovery in speech," *IEEE Transactions on Audio, Speech, and Language Processing*, vol. 16, pp. 186–197, Jan 2008.

[36] "Specification for rfid air interface epc radio-frequency identity protocols class-1 generation-2 uhf rfid protocol for communications at 860 mhz–960 mhz." http://bit.ly/2gem5Ie, 2017. [Online] Last Accessed : 07/12/2017.

[37] "ipod click wheel." http://bit.ly/2gfTW2z, 2017. [Online] Last Accessed : 07/12/2017.

[38] "Alien 9613 higgs-3 loop near-field rfid tag." https://www.atlasrfidstore.com/alien-sit-rfid-white-wet-inlay-aln-9613-higgs-3/, 2017. [Online] Last Accessed : 07/12/2017.

[39] K. V. S. Rao, P. V. Nikitin, and S. F. Lam, "Antenna design for uhf rfid tags: a review and a practical application," *IEEE Transactions on Antennas and Propagation*, vol. 53, pp. 3870–3876, Dec 2005.

[40] N. Ma and L. Chen, "The design of folded dipole antenna," in *2008 4th International Conference on Wireless Communications, Networking and Mobile Computing*, pp. 1–3, Oct 2008.

[41] "Rfid coil antennas." http://bit.ly/2h8wLZI, 2017. [Online] Last Accessed : 07/12/2017.

[42] M. Deng and D. Campbell-Wilson, "The cloverleaf antenna: A compact wide-bandwidth dual-polarization feed for chime," in *2014 16th International Symposium on Antenna Technology and Applied Electromagnetics (ANTEM)*, pp. 1–2, July 2014.

[43] "Opencv python 3.1.0.3." https://pypi.python.org/pypi/opencv-python, 2017. [Online] Last Accessed : 07/12/2017.

[44] "Monza r6 datasheet." https://support.impinj.com/hc/en-us/articles/202765328-Monza-R6-Product-Datasheet, 2017. [Online] Last Accessed : 07/12/2017.

[45] "Thinkmagic rfid redaer." http://bit.ly/2tZeZ3w, 2017. [Online] Last Accessed : 07/12/2017.

[46] L. Du, "An overview of mobile capacitive touch technologies trends," *CoRR*, vol. abs/1612.08227, 2016.

[47] "Microsoft pixelsense - higher than 4k resolution." https://www.microsoft.com/en-us/surface/devices/surface-studio/innovation, 2017. [Online] Last Accessed : 07/12/2017.

[48] A. P. Sample, D. J. Yeager, P. S. Powledge, and J. R. Smith, "Design of a passively-powered, programmable sensing platform for uhf rfid systems," in *2007 IEEE International Conference on RFID*, pp. 149–156, March 2007.

[49] P. Asadzadeh, L. Kulik, and E. Tanin, "Gesture recognition using rfid technology," *Personal Ubiquitous Comput.*, vol. 16, pp. 225–234, Mar. 2012.

[50] S. Amendola, L. Bianchi, and G. Marrocco, "Movement detection of human body segments: Passive radio-frequency identification and machine-learning technologies.," *IEEE Antennas and Propagation Magazine*, vol. 57, pp. 23–37, June 2015.

[51] J. Han, H. Ding, C. Qian, W. Xi, Z. Wang, Z. Jiang, L. Shangguan, and J. Zhao, "Cbid: A customer behavior identification system using passive tags," *IEEE/ACM Transactions on Networking*, vol. 24, pp. 2885–2898, Oct 2016.

[52] L. Shangguan, Z. Zhou, X. Zheng, L. Yang, Y. Liu, and J. Han, "Shopminer: Mining customer shopping behavior in physical clothing stores with cots rfid devices," in *Proceedings of the 13th ACM Conference on Embedded Networked Sensor Systems*, SenSys '15, (New York, NY, USA), pp. 113–125, ACM, 2015.

[53] L. Shangguan and K. Jamieson, "Leveraging electromagnetic polarization in a two-antenna motion tracking system," *ACM CoNext*, 2016.
[54] Q. Lin, L. Yang, Y. Sun, T. Liu, X. Y. Li, and Y. Liu, "Beyond one-dollar mouse: A battery-free device for 3d human-computer interaction via rfid tags," in *2015 IEEE Conference on Computer Communications (INFOCOM)*, pp. 1661–1669, April 2015.
[55] S. Sarkka, V. V. Viikari, M. Huusko, and K. Jaakkola, "Phase-based uhf rfid tracking with nonlinear kalman filtering and smoothing," *IEEE Sensors Journal*, vol. 12, pp. 904–910, May 2012.
[56] G. Marrocco and F. Amato, "Self-sensing passive rfid: From theory to tag design and experimentation," in *2009 European Microwave Conference (EuMC)*, pp. 001–004, Sept 2009.
[57] S. Amendola, G. Bovesecchi, A. Palombi, P. Coppa, and G. Marrocco, "Design, calibration and experimentation of an epidermal rfid sensor for remote temperature monitoring," *IEEE Sensors Journal*, vol. 16, pp. 7250–7257, Oct 2016.
[58] S. Milici, S. Amendola, A. Bianco, and G. Marrocco, "Epidermal rfid passive sensor for body temperature measurements," in *2014 IEEE RFID Technology and Applications Conference (RFID-TA)*, pp. 140–144, Sept 2014.
[59] R. Bhattacharyya, C. Floerkemeier, and S. Sarma, "Rfid tag antenna based sensing: Does your beverage glass need a refill?," in *2010 IEEE International Conference on RFID (IEEE RFID 2010)*, pp. 126–133, April 2010.
[60] S. Manzari, A. Catini, G. Pomarico, C. D. Natale, and G. Marrocco, "Development of an uhf rfid chemical sensor array for battery-less ambient sensing," *IEEE Sensors Journal*, vol. 14, pp. 3616–3623, Oct 2014.
[61] S. Manzari, C. Occhiuzzi, S. Nawale, A. Catini, C. D. Natale, and G. Marrocco, "Humidity sensing by polymer-loaded uhf rfid antennas," *IEEE Sensors Journal*, vol. 12, pp. 2851–2858, Sept 2012.
[62] C. Occhiuzzi, A. Rida, G. Marrocco, and M. Tentzeris, "Rfid passive gas sensor integrating carbon nanotubes," *IEEE Transactions on Microwave Theory and Techniques*, vol. 59, pp. 2674–2684, Oct 2011.
[63] M. Philipose, J. R. Smith, B. Jiang, A. Mamishev, S. Roy, and K. Sundara-Rajan, "Battery-free wireless identification and sensing," *IEEE Pervasive Computing*, vol. 4, pp. 37–45, Jan 2005.
[64] D. Avrahami and S. E. Hudson, "Forming interactivity: A tool for rapid prototyping of physical interactive products," in *Proceedings of the 4th Conference on Designing Interactive Systems: Processes, Practices, Methods, and Techniques*, 2002.
[65] N. Marquardt, A. S. Taylor, N. Villar, and S. Greenberg, "Rethinking rfid: Awareness and control for interaction with rfid systems," in *Proceedings of the SIGCHI Conference on Human Factors in Computing Systems*, CHI '10, (New York, NY, USA), pp. 2307–2316, ACM, 2010.